Eur Biophys J (1998) 27: 153–165

ARTICLE

Thomas Hermann · Pascal Auffinger · Eric Westhof

Molecular dynamics investigations of hammerhead ribozyme RNA

Received: 1 September 1997 / Accepted: 27 November 1997

Abstract The hammerhead ribozyme, a small catalytic RNA molecule, cleaves, in the presence of magnesium ions, a specific phosphodiester bond within its own backbone, leading to 2′3′-cyclic phosphate and 5′-OH extremities. In order to study the dynamical flexibility of the hammerhead RNA, we performed molecular dynamics simulations of the solvated crystal structure of an active hammerhead ribozyme, obtained after flash-freezing crystals soaked with magnesium. Because of a careful equilibration protocol and the use of the Ewald summation in calculating the electrostatic interactions, the RNA structure remained close to the crystal structure, as attested by a root-mean-square deviation below 2.5 Å after 750 ps of simulation. All Watson-Crick base pairs were intact at the end of the simulations. The tertiary interactions, such as the sheared G · A pairs and the U-turn, important for the stabilisation of the three-dimensional RNA fold, were also retained. The results demonstrate that molecular dynamics simulations can be successfully used to investigate the dynamical behaviour of a ribozyme, thus, opening a road to study the role of transient structural changes involved in ribozyme catalysis.

Key words AMBER · Ewald summation · Sheared GA pair · Magnesium ions · Ribose pucker flip

Introduction

The hammerhead ribozyme was originally identified as an RNA motif catalysing the self-cleavage of satellite RNAs in plant viruses and viroids (Symons 1992). The minimal sequence of the hammerhead RNA required for catalysis comprises around 40 nucleotides folded into three stems which are connected by single-stranded regions (Fig. 1a) (Uhlenbeck 1987; for review see Scott and Klug 1996; Thomson et al. 1996). The three-dimensional structure of the hammerhead ribozyme has been determined by X-ray crystal analyses and fluorescence resonance energy transfer techniques (Fig. 1b) (Pley et al. 1994; Scott et al. 1995, 1996; Tuschl et al. 1994). Catalysis of the hammerhead cleavage reaction requires the presence of divalent cations such as Mg^{2+} (Dahm and Uhlenbeck 1991). In the cleavage reaction a hydroxide ion bound to a divalent metal ion deprotonates the cleavage-site 2′-OH group which then attacks the adjacent 3′-phosphate (Fig. 1c) (Dahm et al. 1993). A second divalent metal ion may stabilize the pentacoordinated phosphorous transition state (Scott et al. 1996). Crystal structure analysis revealed the positions of five Mg^{2+} ions bound to an active hammerhead ribozyme (Fig. 1b) captured by flash-freezing RNA crystals after soaking with Mg^{2+} at pH 8.5 where the ribozyme cleaves in the crystal at room temperature (Scott et al. 1996). One of the Mg^{2+} ions (site 6) is directly bound to the cleavable phosphate and is thus considered part of the active site of the ribozyme. A second Mg^{2+} ion (site 1) is located 4.25 Å apart from $Mg^{2+}_{(6)}$. A shortcoming of the hammerhead RNA crystal analyses available to date is the fact that in neither of the structures is the cleavage-site 2′-hydroxyl in a favourable position for nucleophilic attack at the adjacent phosphate (McKay 1996). To initiate the cleavage reaction, a conformational change in the hammerhead RNA is therefore likely (Scott et al. 1996; Mei et al. 1989; Setlik et al. 1995; Hermann et al. 1997).

It is the aim of the present work to study the dynamical flexibility of the hammerhead RNA using molecular dynamics (MD) simulation techniques in order to rationalize conformational changes in the RNA which could help to build a structurally consistent mechanistic model for hammerhead ribozyme cleavage. Starting from the crystal structure of an active hammerhead ribozyme, we performed MD simulations of the hammerhead RNA in the presence of explicit solvent and salt ions.

Based on work presented at the 2nd European Biophysics Congress, Orléans, France, July 1997

T. Hermann · P. Auffinger · E. Westhof (✉)
Institut de Biologie Moléculaire et Cellulaire du CNRS,
15 Rue René Descartes, F-67084 Strasbourg, France
(e-mail: westhof@ibmc.u-strasbg.fr)

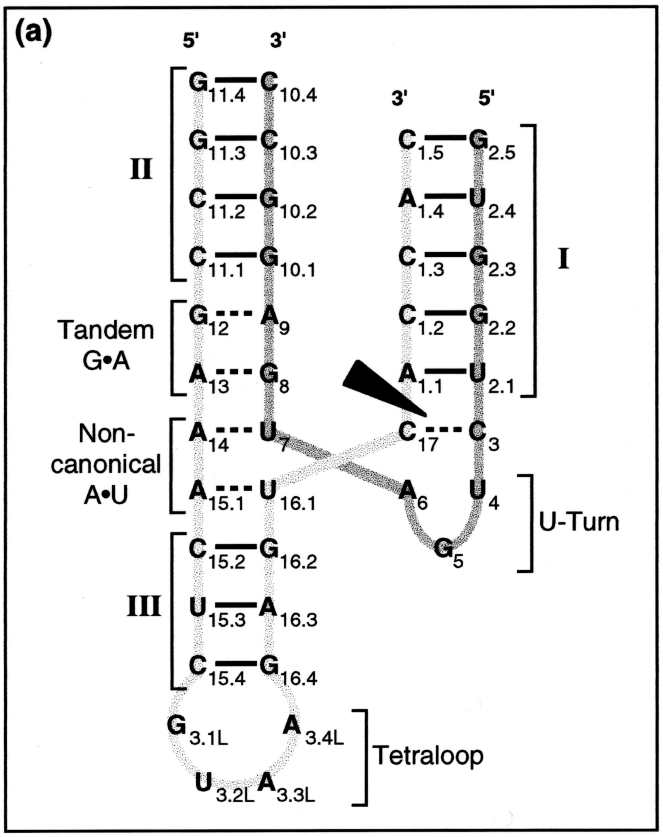

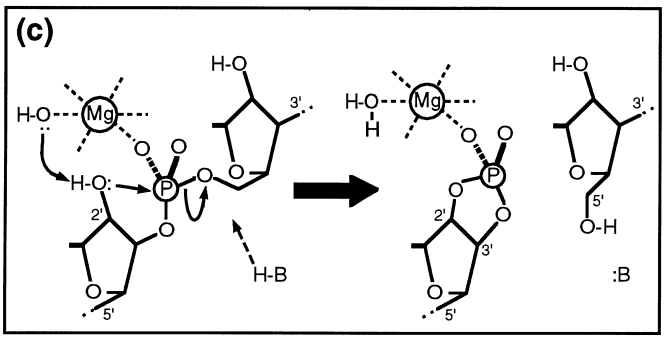

Fig. 1 **a** Secondary structure of the hammerhead RNA emphasizing the continuous stacking of stems II and III with the connecting region consisting of two sheared G · A tandem base pairs and two non-canonical A · U pairs. The site of catalytic cleavage between C_{17} and $A_{1.1}$ on stem I is indicated by an arrow. Stem I connects to stem II via the U-turn U_4 to A_6. **b** Three-dimensional folding of the hammerhead RNA as determined by crystal structure analysis after flash-freezing crystals of an active hammerhead ribozyme in the presence of Mg^{2+} ions (Scott et al. 1996). The positions of five Mg^{2+} ions (1–4, 6) are shown as spheres. $Mg^{2+}_{(6)}$ is directly bound to the pro-R_P oxygen of the cleavable phosphate (*arrow*). **c** General mechanism previously proposed for the hammerhead catalytic cleavage (Dahm et al. 1993; for review see Thomson et al. 1996). Hydroxide coordinated to a Mg^{2+} ion that is bound to the cleavable phosphate activates the cleavage-site 2′-OH group, which then attacks the adjacent 3′-phosphate. An additional acidic group (H-B) donates a proton in the reaction. The products of cleavage are 2′3′-cyclic phosphate and 5′-OH ends

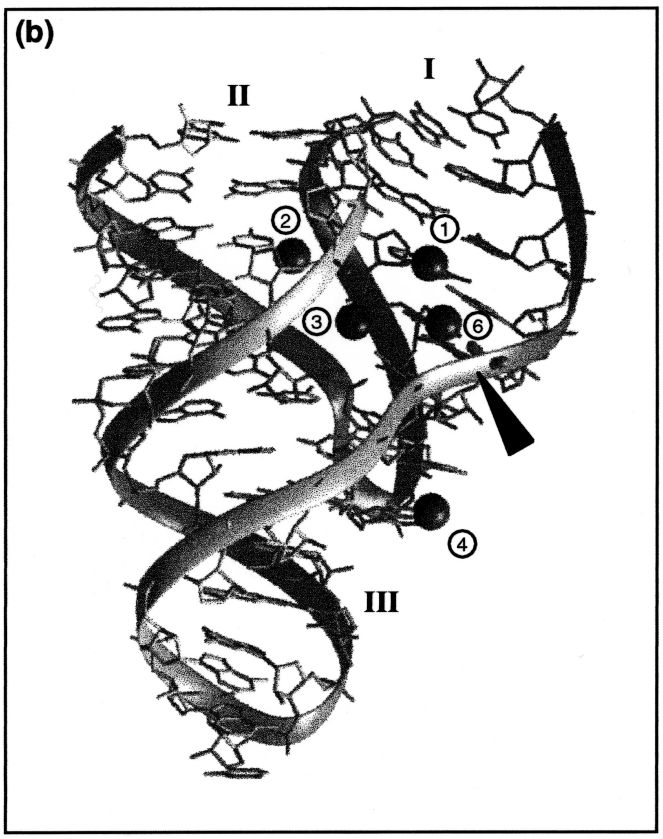

We have previously reported results from MD simulations (Hermann et al. 1997) suggesting that in the hammerhead ribozyme a μ-bridging OH^- ion is located between two Mg^{2+} ions close to the cleavable phosphate. In an attempt to uncover pathways from the ground state structure of the hammerhead in the crystal towards an RNA conformation where the cleavage reaction is sterically possible, we have also performed constrained simulations. These simulations allowed us to show that a flip from the C3′-endo to the C2′-endo conformation of the ribose at the cleavable phosphate is sufficient to position the 2′-hydroxyl group, the attacking nucleophile in the cleavage reaction, in proximity to both the attacked phosphorous atom and the activating μ-bridging OH^- ion. Thus, the simulations have led to new insight into the mechanism of hammerhead ribozyme cleavage (Hermann et al. 1997).

Here, we report in detail the dynamical behaviour of important geometrical, stereochemical, and conformational parameters characterising the hammerhead three-dimensional RNA fold.

Methods

All calculations were performed on a Silicon Graphics Indigo^2 IMPACT 10000 workstation using the AMBER4.1 software (Pearlman et al. 1994) and force field (Cornell et al. 1995). Additional force field parameters for Mg^{2+} ions were from Åqvist (1990), those for OH^- from Lee et al.

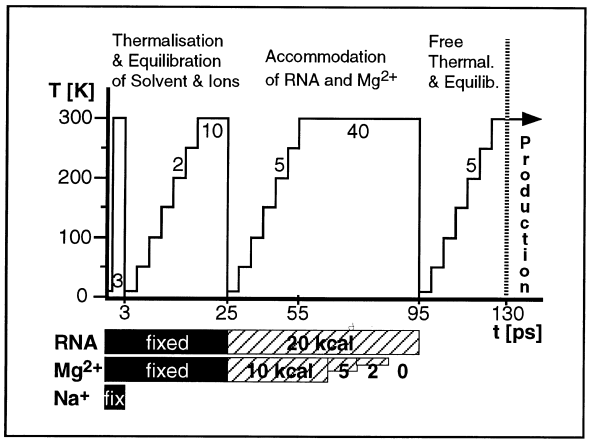

Fig. 2 Equilibration protocol used for the accommodation of solvent and ions around the hammerhead crystal structure. The numbers give the simulation time in ps at a given temperature. *Horizontal bars* at the bottom indicate the periods where constraints or energetical restraints (in kcal) were imposed for tethering RNA and ions. For details see the Methods section

(1995). Atomic coordinates of the hammerhead RNA were from a previously published crystal structure analysis of an active hammerhead ribozyme freeze-trapped after soaking crystals with Mg^{2+} ions at pH 8.5 (Scott et al. 1996).

The solvated system was prepared by placing the RNA in a rectangular box (~75×62×48 $Å^3$) of SPC/E water (Berendsen et al. 1987) typically containing ~6500 solvent molecules. A salt concentration of 380 mM Na^+ and 140 mM Cl^- was achieved by adding 50 Na^+ and 18 Cl^- ions, placed with the PROION program of the GROMOS package (van Gunsteren and Berendsen 1987), according to the electrostatic potential around the solute such that no ion was closer than 4.5 Å to any solute atom.

The MD simulations were run at a time step of 2 fs using the SHAKE algorithm (Ryckaert et al. 1977) to constrain the X–H bond lengths. A constant temperature of 298 K and a constant pressure of 1 atm were maintained by coupling to an external heat bath every 0.4 ps and volume scaling every 0.5 ps (Berendsen et al. 1984). Van der Waals interactions were truncated at 9.0 Å, while no cutoff was applied on the electrostatic term. The electrostatic interactions were calculated with the Particle Mesh Ewald method (Darden et al. 1993) with a charge grid spacing close to 1.0 Å.

An equilibration protocol was devised to ensure careful accommodation of solvent and ions around the crystal structure of the RNA (Fig. 2). Starting from a solvent box built with the AMBER package, 3 ps of water equilibration at 298 K were calculated with all ions and RNA fixed, followed by a restart at 10 K and heating to 298 K in steps of 50 K, with 2 ps of simulation at each temperature, where water, Na^+ and Cl^- ions were allowed to move. After 10 ps at 298 K a restart at 10 K was performed while the RNA atoms except for hydrogen were constrained with 20 kcal and Mg^{2+} ions with 10 kcal to their positions in the crystal structure. The system was heated to 298 K in steps of 50 K with 5 ps of simulation at each temperature. Subsequently the constraint on the Mg^{2+} ions was gradually lowered to zero during 40 ps simulation at 298 K. Finally, after a restart at 10 K, the system was again heated to 298 K in 5 ps steps of 50 K without applying any constraints.

For simulations at 350 K, gradual heating in steps of 10 K, with 10 ps calculation at each temperature, was performed, starting from atom coordinates and velocities of a configuration within a 300 K trajectory.

During the productive MD phase, coordinates were recorded for analysis every 0.5 ps. Visualisation of the trajectories was done with the MDDRAW software (Engler and Wipff 1994).

Results and discussion

Before focusing on the behaviour of the ribozyme during the MD simulations, we will first briefly summarize the binding and coordination of Mg^{2+} ions to the hammerhead RNA, owing to their importance in the structuration and folding of RNA in general (for a review see Brion and Westhof 1997).

Behaviour of the Mg^{2+} ions during the MD simulations

The positions of five Mg^{2+} ions were determined in the crystal structure analysis of an active hammerhead ribozyme captured by flash-freezing crystals in the presence of Mg^{2+} at pH 8.5 (Fig. 1b) (Scott et al. 1996). In order to ensure an optimal hydration of the metal ions at their binding sites, an elaborate equilibration procedure was used at the beginning of the MD simulations. After a phase where the RNA and the Mg^{2+} ions were fixed to their positions in the crystal structure, and only solvent water was allowed to move, the tethering of the Mg^{2+} ions was gradually released while the RNA was still constrained. During the last phase of the equilibration protocol, namely heating from 10 K to the final simulation temperature of 298 K, no constraints were imposed on the system.

The Mg^{2+} ion at site 6 remained in all simulations stably bound to the pro-R_P oxygen of the cleavable phosphate. In contrast, in a first set of calculations, the Mg^{2+} ion at site 1, located in proximity to $Mg^{2+}_{(6)}$, moved rapidly away from its original position in the crystal structure as soon as the constraints were released (Fig. 3a). Further calculations provided evidence that this destabilisation of $Mg^{2+}_{(1)}$ is due to a repulsive electrostatic interaction with $Mg^{2+}_{(6)}$ in the neighborhood (Hermann et al. 1997). Thus, when simulations were performed on the hammerhead crystal structure without a Mg^{2+} ion at site 6, resembling the situation found in crystals obtained at pH 5.0 (Scott et al. 1996), $Mg^{2+}_{(1)}$ stayed close to its original position. In this case, a water molecule occupied the metal binding site 6. However, $Mg^{2+}_{(1)}$ could be stabilized in the presence of $Mg^{2+}_{(6)}$ by introducing a μ-bridging OH^- ion which replaces a water molecule between these two metals (Fig. 3b). The stabil-

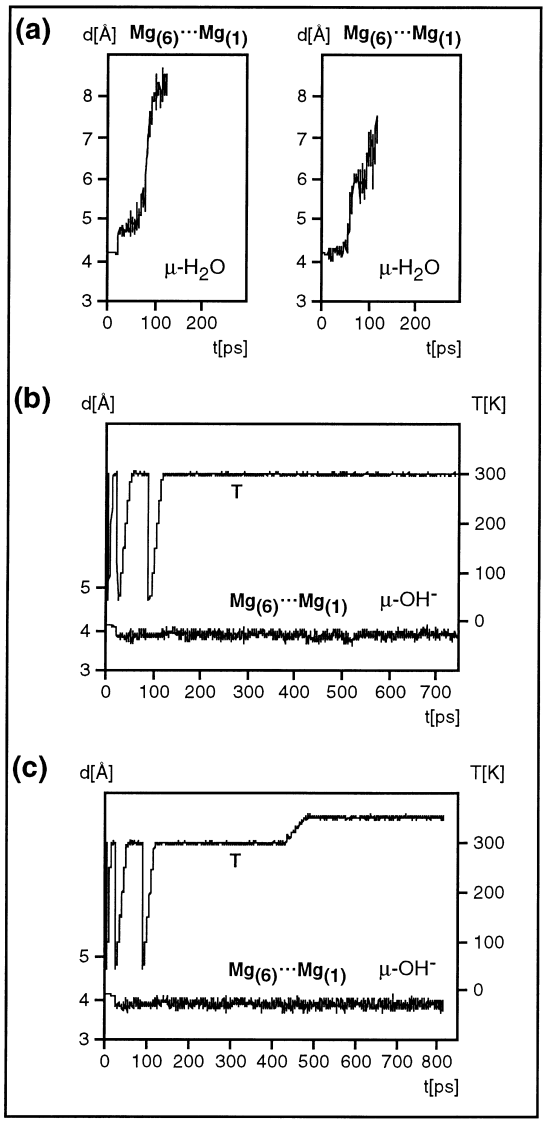

Fig. 3a–c Distance between the Mg^{2+} ions at sites 6 and 1 in the hammerhead RNA during MD simulations performed using various assumptions. **a** In all simulations with a bridging water molecule (μ-H_2O) between $Mg^{2+}_{(6)}$ and $Mg^{2+}_{(1)}$, rapid dissociation of the Mg^{2+} ion from site 1 was observed. Shown are inter-Mg^{2+} distances recorded in a simulation with all five Mg^{2+} ions (*left panel*) and in a simulation where the metal at site 2 was omitted (*right panel*). **b** When the water molecule between $Mg^{2+}_{(6)}$ and $Mg^{2+}_{(1)}$ was replaced by a μ-bridging OH^- ion, the metal at site 1 was stabilised and stayed close to its binding position in the crystal structure, as indicated by the constant distance between $Mg^{2+}_{(6)}$ and $Mg^{2+}_{(1)}$. The curve on top shows the temperature of the system during the simulation (*right ordinate*). **c** The μ-hydroxo-bridged metal cluster was stable even at elevated temperatures as shown by the distance plot recorded for a MD simulation where the temperature (*top curve*) was increased to 350 K after 430 ps of calculation at 298 K

ity of the μ-hydroxo-bridged metal cluster is attested by the fact that the cluster was stable even at a simulation temperature of 350 K (Fig. 3c). The proposition of a μ-bridging OH^- ion is in line with the observation of continous electron density between $Mg^{2+}_{(1)}$ and $Mg^{2+}_{(6)}$, as described previously (Scott et al. 1996). It was suggested that the μ-hydroxo-bridged metal cluster activates the cleavage-site 2′-OH for nucleophilic attack at the cleavable phosphate (Hermann et al. 1997).

While $Mg^{2+}_{(1)}$ and $Mg^{2+}_{(6)}$ are close to the cleavable phosphate, the Mg^{2+} ion at site 3 is 11 Å away and, thus, is probably not involved in the catalytic reaction but in stabilizing the U-turn between helices I and II. During the MD simulations, $Mg^{2+}_{(3)}$ stayed bound to the RNA where it is held by hydration waters forming hydrogen bridges with the phosphates of U_7 and G_8, respectively, and with O4 of the $U_{2.1}$ side chain (Scott et al. 1996; Hermann et al. 1997). The distance between $Mg^{2+}_{(3)}$ and the cleavable phosphate did not change significantly in the calculations.

The Mg^{2+} ion at site 2 is the metal most distant from the cleavage site (15 Å). However, like the cations at sites 1, 3 and 6, it is located within the cavity formed by the facing deep grooves of stems I and II. In the hydrated hammerhead RNA, $Mg^{2+}_{(2)}$ makes contacts mediated by water molecules of the metal hydration shell to O2′ of G_8 and to N4 of $C_{11.2}$. These interactions remained intact during the MD simulations. Also, a long-ranging contact via two water molecules to the phosphate group of A_9 was present. Thus, as was observed for $Mg^{2+}_{(3)}$, $Mg^{2+}_{(2)}$ stayed stably bound to the hammerhead ribozyme during the calculations solely by interactions of the hydration shell of the metal with the RNA.

A fifth metal ion, $Mg^{2+}_{(4)}$, is found at an unusual position close to the base of the highly conserved G_5 within the U-turn. Favourable interactions between this cation and the RNA could not be envisaged and, indeed, $Mg^{2+}_{(4)}$ dissociated from its original position during all MD simulations. No long-lived hydrogen bonds between the hydration water of $Mg^{2+}_{(4)}$ and the RNA were observed. While the simulations offer no clue as to the role of $Mg^{2+}_{(4)}$, one might suggest that the release of this ion is required for facilitating the catalytic reaction. Interestingly, dissociation of Mg^{2+} ions from the hammerhead RNA during cleavage was observed experimentally (Long et al. 1995).

Behaviour of the hammerhead RNA during the MD simulations

Global features of the hammerhead structure

Only minor distortions of the crystallographically determined three-dimensional RNA structure were observed during the MD simulations following the use of both the Ewald summation for calculating the electrostatic interactions and the careful equilibration protocol that was employed for accommodating solvent and ions around the ribozyme. The global RMS deviation between the simulated and the crystal structure was of the order of 2.5 Å after 750 ps of calculation at 298 K (Fig. 4a). In a different simulation where the temperature was raised to 350 K (75°C), the system did not stabilize and the RMS deviation increased continuously (Fig. 4a) probably due to thermal unfolding of the RNA structure. However, a detailed analy-

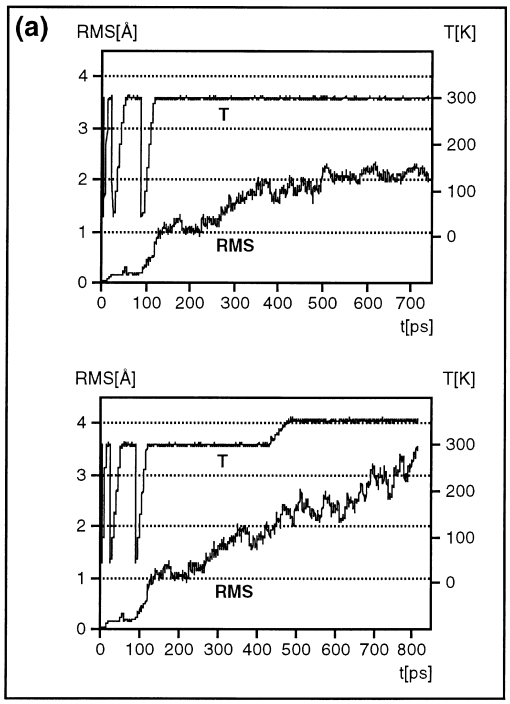

Fig. 4a, b RMS deviation of the hammerhead RNA during various MD simulations compared to the crystal structure coordinates. **a** Owing to a careful equilibration protocol, the RMS deviation of the RNA was of the order of 2.5 Å after 750 ps of calculation (*top panel*). The inserted curve on top shows the temperature of the system (*right ordinate*). In a simulation where the temperature was increased to 350 K after 430 ps at 298 K, the RMS deviation did not stabilise (*bottom panel*). **b** Maximum RMS deviations during a 750 ps simulation at 298 K calculated separately for each nucleotide of the ribozyme. In the top panel, the regions of stems I–III, the U-turn (U) and the tetraloop (T) are indicated. The *bottom panel* shows the secondary structure of the hammerhead where the RMS deviation of single nucleotides is coded in four ranges by different patterns as indicated in the inserted legend. The cleavage site is indicated by an arrow

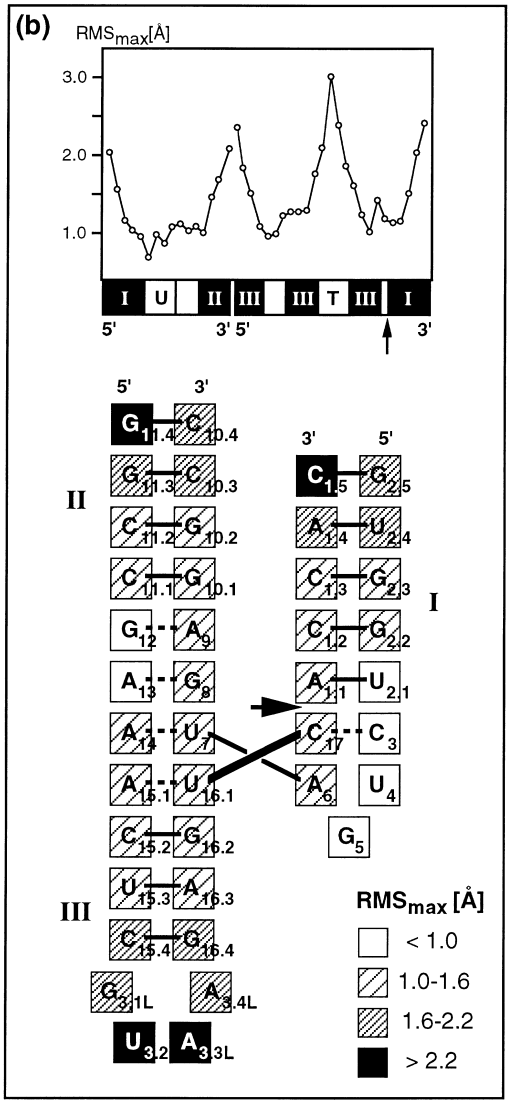

sis of the structural changes in the RNA during the simulation at 350 K would be beyond the scope of this work. Melting of the hammerhead RNA structure is observed experimentally at temperatures above 60°C (Takagi and Taira 1995).

Analysis of the maximal RMS deviation during the 750 ps simulation calculated separately for each nucleotide (Fig. 4b) revealed three regions with noteworthy distortions, namely at the extremities of stems I and II and within the tetraloop on stem III ($U_{3.2L}$, $A_{3.3L}$). This finding is not surprising since helix ends and loops are regions of obvious intrinsic flexibility, e.g. as observed previously in simulations of RNA hairpin structures (Auffinger and Westhof 1996; Miller and Kollman 1997). In contrast, the loop region of the U-turn displayed a low deviation, probably due to stabilizing tertiary interactions involving nucleotides of this loop (see below).

The observed global deviation of the hammerhead RNA from the crystal structure was essentially due to tilting of

Fig. 5a–g Behaviour of hydrogen bonds in the hammerhead RNA during a 750 ps MD simulation. The start of the productive MD phase after equilibration is marked in each panel by a stippled line. For details see the text. **a** Watson-Crick hydrogen bonds in the G-C closing base pairs of stem I ($G_{2.5}$-$C_{1.5}$) and II ($G_{11.4}$-$C_{10.4}$). **b** Hydrogen bonds in the sheared G · A pairs within the augmented stem II helix. The two inter-base hydrogen bonds appear in both G · A pairs (formula scheme, middle panel). G_{13} · A_8 is additionally stabilised by hydrogen bonds between the exocyclic amino groups of both G and A to the backbone of the other base (fine stippled lines). In G_{12} · A_9 a single additional bond from the adenine to the furanose O4′ of G appears (coarse stippled line). The dynamical behaviour of the hydrogen bonds reveals an in-plane breathing motion of the adenine (arrow), with the pivotal axis (black dot) perpendicular to the stable $G_{N2-H\cdots N7}A$ bond. **c** Hydrogen bonds in the two non-canonical A · U pairs within the augmented stem II helix. **d** Interactions of the $U_{16.1}$ 2′-OH group that switches (dashed line) between two hydrogen bond acceptors among them the furanose oxygen of the cleavage-site nucleotide C_{17}. **e**, **f** Tertiary interactions of nucleotides within the augmented stem II helix and the U-turn. **g** Hydrogen bonds within the GUAA tetraloop closing stem III

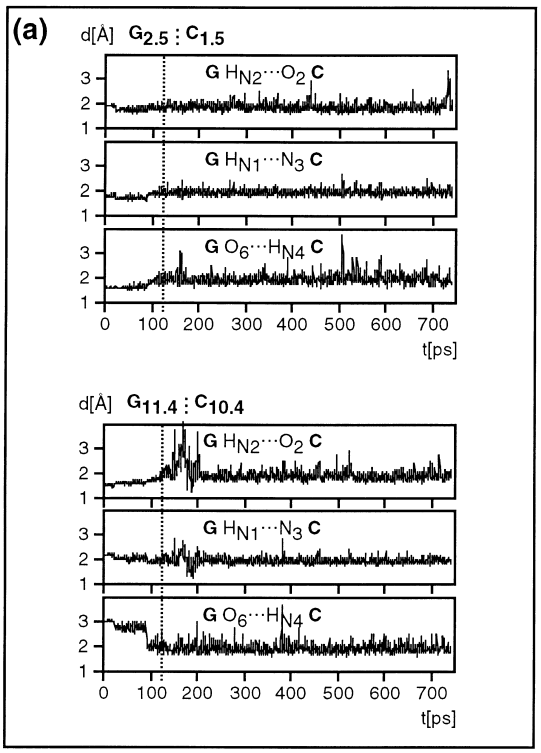
(a)
d[Å] G2.5 : C1.5
G HN2···O2 C
G HN1···N3 C
G O6···HN4 C
0 100 200 300 400 500 600 700
t[ps]
d[Å] G11.4 : C10.4
G HN2···O2 C
G HN1···N3 C
G O6···HN4 C
0 100 200 300 400 500 600 700
t[ps]

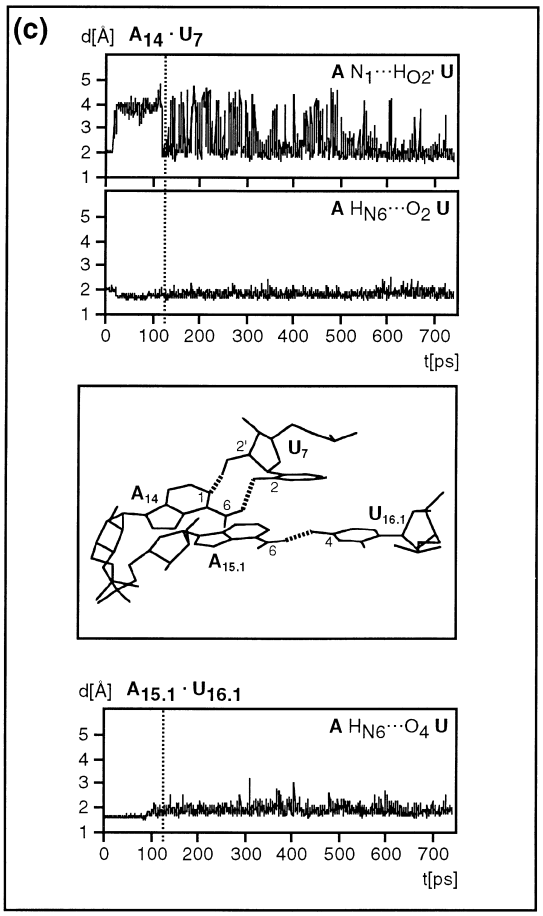
(c)
d[Å] A14 · U7
A N1···HO2' U
A HN6···O2 U
0 100 200 300 400 500 600 700
t[ps]
U7
A14
U16.1
A15.1
d[Å] A15.1 · U16.1
A HN6···O4 U
0 100 200 300 400 500 600 700
t[ps]

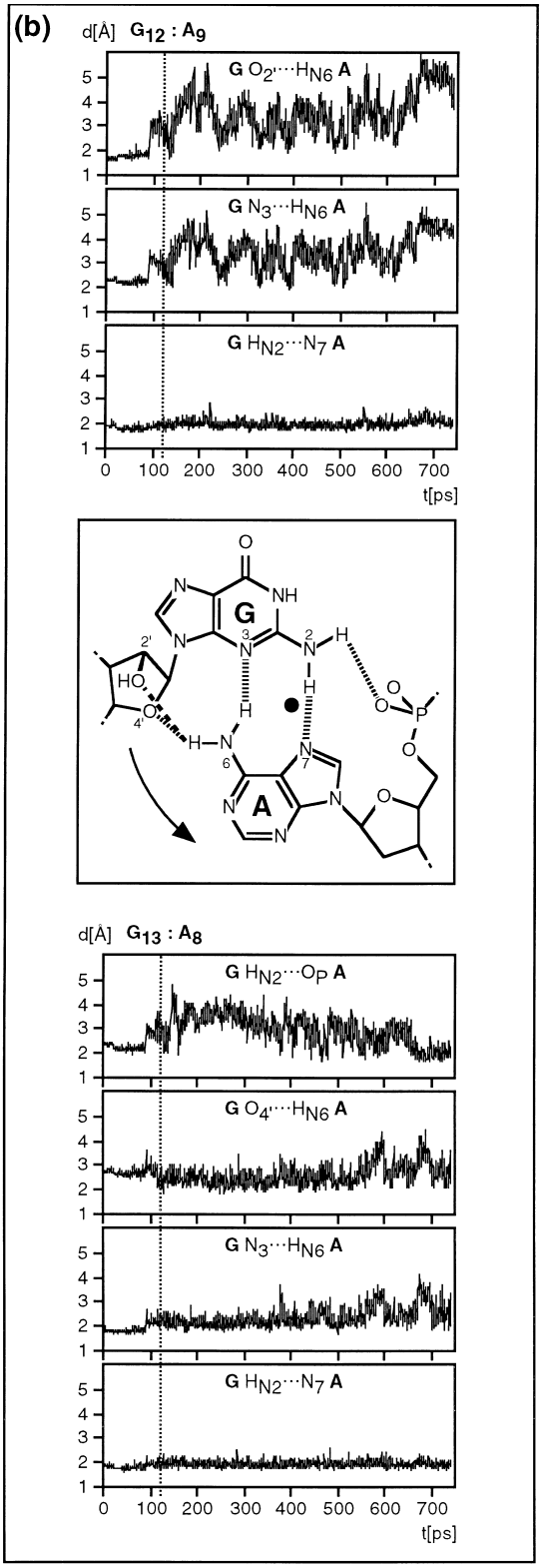
(b)
d[Å] G12 : A9
G O2'···HN6 A
G N3···HN6 A
G HN2···N7 A
0 100 200 300 400 500 600 700
t[ps]
G
A
d[Å] G13 : A8
G HN2···OP A
G O4'···HN6 A
G N3···HN6 A
G HN2···N7 A
0 100 200 300 400 500 600 700
t[ps]

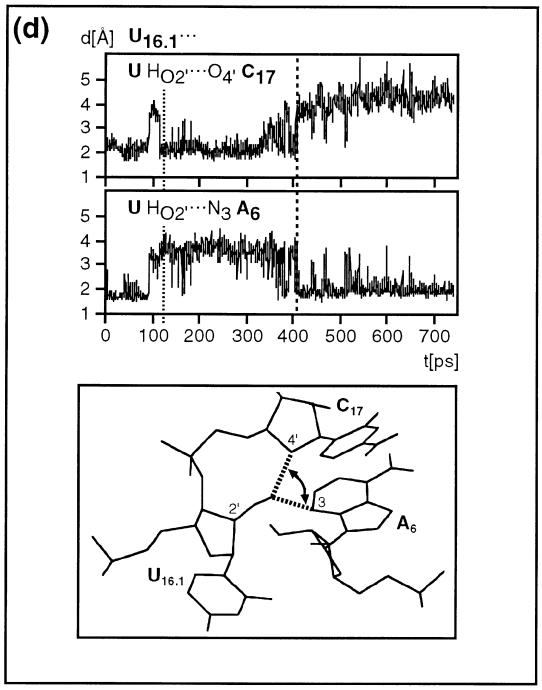
(d)
d[Å] U16.1···
U HO2'···O4' C17
U HO2'···N3 A6
t[ps]
C17
4'
2'
3
A6
U16.1

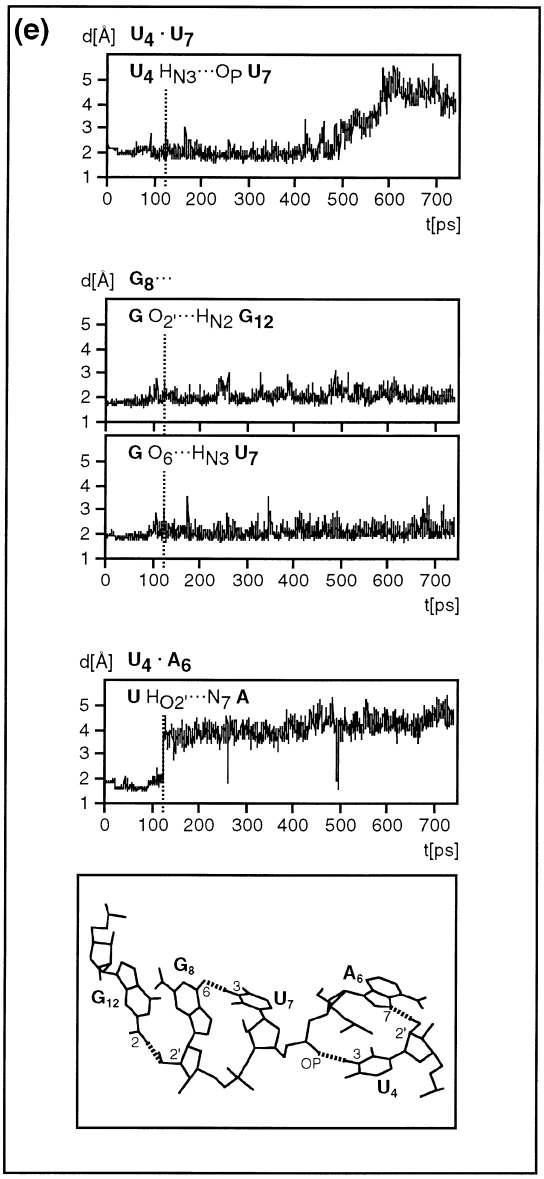
(e)
d[Å] U4 · U7
U4 HN3···OP U7
t[ps]
d[Å] G8···
G O2'···HN2 G12
G O6···HN3 U7
d[Å] U4 · A6
U HO2'···N7 A
G8
G12
U7
A6
OP
U4

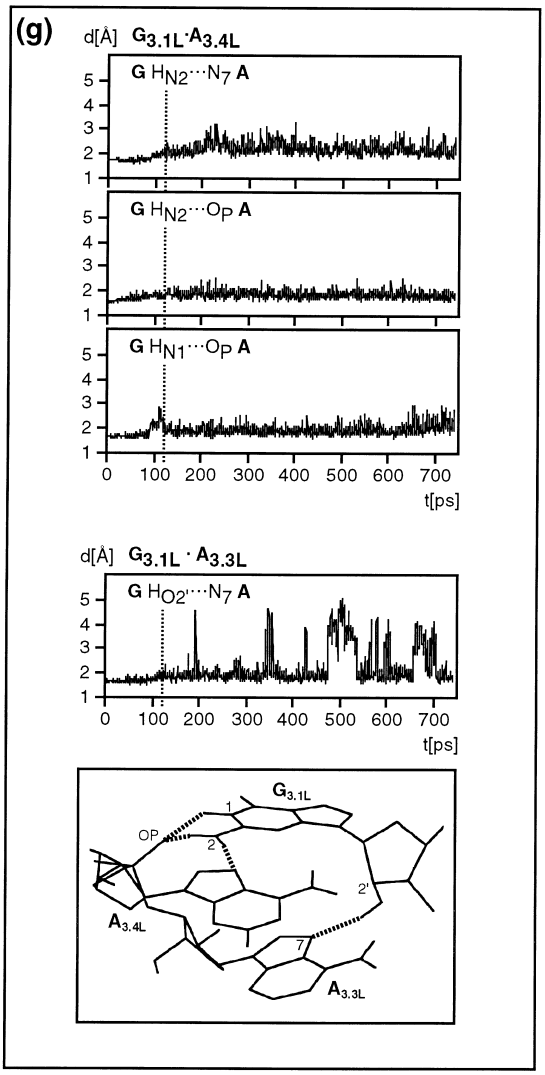
(g)
d[Å] G3.1L·A3.4L
G HN2···N7 A
G HN2···OP A
G HN1···OP A
t[ps]
d[Å] G3.1L · A3.3L
G HO2'···N7 A
G3.1L
OP
A3.4L
A3.3L

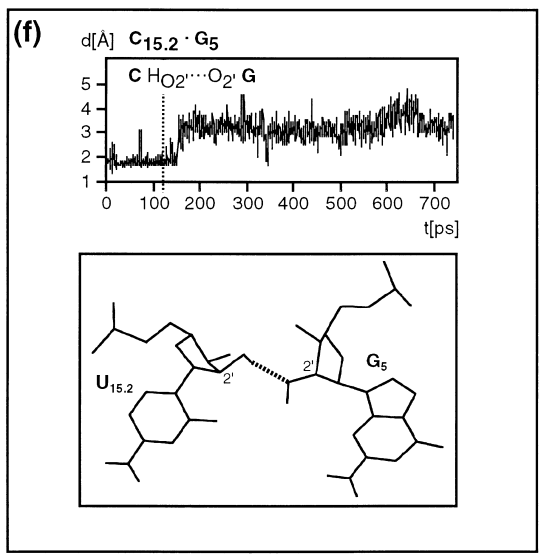
(f)
d[Å] C15.2 · G5
C HO2'···O2' G
t[ps]
U15.2
G5

stems I and II during the simulations. In the crystal structure used as a starting point for the simulations, stems I and II are stabilised in a roughly parallel orientation by the blunt end packing of two hammerhead molecules against each other leading to a pseudocontinuous helical packing scheme (Scott et al. 1996) frequently observed for nucleic acid helices (Wahl and Sundaralingam 1995; Masquida and Westhof 1997). In the MD simulations, only a single hammerhead molecule is included and, thus, tilting of stems I and II due to the absence of the crystal contacts is not surprising. Similarly, in crystals of a different RNA/DNA hammerhead construct, a packing scheme without contacts between stem ends occurs and, consequently, stems I and II are tilted (Pley et al. 1994).

Stability of the secondary structure and of the tertiary interactions in the hammerhead RNA

The hammerhead RNA fold used in the simulations contains three stems totaling 12 Watson-Crick base pairs (Fig. 1a). Although no constraints were imposed on the hydrogen bonds, all base pairs remained intact during the MD simulations, as illustrated by the stable hydrogen-bonding pattern of the critical closing base pairs at extremities of stems I and II (Fig. 5a). Interestingly, the $G_{O6\cdots H-N4}C$ hydrogen bond within the $G_{11.4}$-$C_{10.4}$ pair that was absent at the beginning of the simulation, owing to an unfavourable geometry in the crystal structure, formed readily during the equilibration phase when the constraints tethering the RNA to the X-ray structure were released (Fig. 5a).

Stems II and III are coaxially stacked and connected by four non-canonical base pairs, i.e. a tandem of sheared G · A pairs ($G_8 \cdot A_{13}$, $G_{12} \cdot A_9$) and two non-Watson-Crick A · U pairs ($A_{14} \cdot U_7$, $A_{15.1} \cdot U_{16.1}$) (Fig. 1a) (Pley et al. 1994; Scott et al. 1995). For both G · A pairs, the hydrogen bonds involving the Hoogsteen positions of adenine are stable during the MD simulations (Fig. 5b). However, the hydrogen bond between the exocyclic N6 amino group of adenine and N3 of guanine shows fluctuations, leading to transient bond breaking in the case of $G_{12} \cdot A_9$. The interaction between N6(A_9) with 2′-OH of G_{12} is not stable, whereas the corresponding hydrogen bond between N6(A_{13}) and O4′(G_8), although labile, remains intact.

A hydrogen bond, observed in the X-ray structure, between the phosphate of A_{13} and the exocyclic N2 amino group of G_8, dissociated during the equilibration procedure but formed again after 650 ps of simulation. Summarizing the dynamical behaviour of the hydrogen bonds in the G · A pairs, an in-plane breathing motion of the adenine bases is revealed, with the pivotal axis perpendicular to the stable $G_{N2-H\cdots N7}A$ bond (Fig. 5b). Overall, the sheared $G_8 \cdot A_{13}$ base pair, which stacks on the single hydrogen bonded non-Watson-Crick $A_{14} \cdot U_7$ pair, appears more stable than the adjacent sheared $G_{12} \cdot A_9$ base pair, which stacks on a standard Watson-Crick pair ($G_{10.1}$-$C_{11.1}$).

In the non-Watson-Crick pairs $A_{14} \cdot U_7$ and $A_{15.1} \cdot U_{16.1}$ a single hydrogen bond occurs, engaging in both cases the exocyclic N6 amino group of the adenine as hydrogen donor, while the uridine acceptor atom is O2 in the $A_{14} \cdot U_7$ pair and O4 in the $A_{15.1} \cdot U_{16.1}$ pair. During the 750 ps simulation, these interactions remain stable in both A · U pairs (Fig. 5c). The $A_{14} \cdot U_7$ pair additionally contains a fluctuating hydrogen bond between the adenine N1 atom and the 2′-OH group of the uridine backbone which forms only transiently during the simulations.

At the core of the hammerhead wishbone structure, several tertiary interactions form between the augmented II/III helix and the U-turn at the basis of stem I containing the catalytic pocket (Pley et al. 1994; Scott et al. 1995). The tertiary interactions involve hydrogen bonds between bases and the sugar phosphate backbone or between sugars. During the MD simulations, these tertiary interactions displayed a more dynamical behaviour than the hydrogen bonds between bases, either Watson-Crick or non-canonical pairs, described above. The interaction between the 2′-OH group of $U_{16.1}$ with N3(A_6) dissociated during the equilibration and a new hydrogen bond between the $U_{16.1}$ 2′-OH group and O4′(C_{17}) was formed (Fig. 5d). However, after 400 ps, the original hydrogen bond between the O2′($U_{16.1}$) and N3(A_6) was restored. Interestingly, the latter hydrogen bond is present only in the crystal structure of the active ribozyme intermediate flash-frozen at pH 8.5 (Scott et al. 1996).

The hydrogen bond between OP(U_7) and N3-H(U_4) within the U-turn, which is also found in the U-turn motif of tRNAs (Quigley and Rich 1976; Westhof et al. 1983), was stable over the first 550 ps of the 750 ps trajectory when it dissociated without the formation of a new compensating interaction (Fig. 5e). In multiple 500 ps MD simulations of $tRNA^{Asp}$ this hydrogen bond remained intact over about the same period (Auffinger and Westhof 1996). The breaking of the $U_{N3-H\cdots ORP}U$ hydrogen bond in the hammerhead simulation is probably linked to the induced flip of the ribose pucker from C3′-endo to C2′-endo of residue A_6 which is observed shortly afterwards (see below).

While a hydrogen bond between the 2′-OH groups of $C_{15.2}$ and G_5, dissociated immediately after the equilibration phase (Fig. 5f), the interactions between, respectively, U_7 and G_{12} and O6(G_8) or O2′(G_8), stabilising the stack of non-canonical G · A and A · U pairs, are stable over 750 ps (Fig. 5e). Among the tertiary interactions in the hammerhead RNA involving 2′-OH groups, the hydrogen bond between O2′(G_8) and N2-H(G_{12}) is the one that displayed the highest stability during the simulations. Finally, the hydrogen bond within the U-turn, between N7(A_6) and O2′(U_4), was not retained (Fig. 5e).

The GUAA tetraloop on top of stem III is stabilised by the sheared base pair $G_{3.1L} \cdot A_{3.4L}$ and an additional hydrogen bond between 2′-OH of $G_{3.1L}$ an the N7 of $A_{3.4L}$ (Pley et al. 1994; Scott et al. 1995). The three hydrogen bonds directed from the base of $G_{3.1L}$ to N7 of the base and to the phosphate of $A_{3.4L}$ remained intact during the MD simulations (Fig. 5g). Another interaction of the $A_{3.3L}$ base and the $G_{3.1L}$ 2′-OH group displayed more dynamical behaviour (Fig. 5g). In summary, the geometry of the GUAA tetraloop is maintained during the simulations despite the

high flexibility of this region (discussed in the following paragraph) and the observation of a relatively large deviation from the crystal structure (see above).

Among the seven hydrogen bonds involving the 2′-OH group, three break early on in the simulation trajectory after the release of the constraints on the RNA. Concerning the other four hydrogen bonds, one appears to alternate between two acceptors ($U_{16.1}$(OH2′) · C_{17}(O4′) or A_6(N3)), two alternate frequently between formation and breakage ($G_{3.1L}$(OH2′) · $A_{3.3L}$(N7) and U_7(OH2′) · A_{14}(N1), and finally one is stable throughout the trajectory (G_8(O2′) · G_{12}(HN2)). In MD simulations of RNA, the stability of hydrogen bonds involving a 2′-OH group is noticeably less than that of other hydrogen bonds, an observation which was attributed to the rotational mobility of the H atom about the C2′-O2′ bond (Auffinger and Westhof 1997).

Conformational flexibility of the hammerhead RNA

The maximal RMS deviation, determined over the whole simulation period separately for each nucleotide of the hammerhead RNA, pointed to three regions with noteworthy deviations from the crystal structure (Fig. 4b). The observed distortions might reflect intrinsic conformational flexibility of the hammerhead RNA. In order to quantify the flexibility of different parts of the ribozyme, we calculated the standard deviation of the RMS deviation (σRMS) for each nucleotide during unconstrained simulation (Fig. 6a). Clearly, a correlation exists between the regions where major distortions of the crystal structure are observed and those regions where a high σRMS value indicates increased local flexibility. Such regions are the extremities of stems I and II and the tetraloop on stem III. The flexibility of the nucleotides at the stem ends differs characteristically within the base pairs (Fig. 6a). The lower flexibility of $G_{2.5}$ and $C_{10.4}$ compared to $G_{11.4}$ and $C_{1.5}$ is due to the location of these nucleotides at the contact interface of the stems which are slightly tilted towards each other.

Low flexibility is observed for the core region of the hammerhead RNA fold comprising nucleotides in the neighborhood of the sheared G · A pairs and the U-turn (Fig. 6a). This finding can be explained by the various tertiary interactions (see above) which are tethering together the hammerhead RNA core.

Comparison of the flexibility calculated from the MD trajectory with experimental data is accomplished by means of the crystallographic thermal parameters (*B*-factors) which are related to atomic RMS deviation (McCammon and Harvey 1987). We calculated the per nucleotide *B*-factors for different time windows during the last 500 ps of the productive phase of the 750 ps simulation and compared them to the *B*-factors from two crystal structures (Scott et al. 1995; Scott et al. 1996) of the hammerhead ribozyme (Fig. 6b). The resulting theoretical *B*-factors did not depend significantly on the chosen time window, i.e. *B*-factors calculated from 200 to 400 ps were close to those calculated for the last 200 ps window. As expected, the stem extremities display a higher mobility during the simulation compared to the RNA in the crystal owing to the absence of the stem blunt end packing (see above). Similarly, higher flexibility in the simulation is observed for the tetraloop involved in crystal packing contacts (Scott et al. 1995) which are lacking in the solution MD calculation. However, we have no explanation for the deviation in *B*-factors for nucleotides around A_9 and A_{14} which display much higher values in the crystal than in the simulation. The continuous stacking scheme that incorporates A_9 and A_{14} between stems II/III and various tertiary interactions in this region argue intuitively against high flexibility in this region. Indeed, the *B*-factors from the MD simulation for nucleotides around A_9 and A_{14} are in satisfying agreement with crystallographical data of a different hammerhead construct (Pley et al. 1994), the core region of which is identical to the hammerhead used for the MD calculations (Fig. 6c). Deviations occur owing to the different position of the tetraloop and to elongated stems. However, as was observed in the simulations, the ribozyme core region also displays low flexibility in this different hammerhead construct.

Despite its low overall flexibility during the simulations, a flip of the ribose pucker from C3′-endo to C2′-endo of residue A_6 occurred spontaneously after 550 ps during a 750 ps MD simulation (Fig. 6d). This conformational change is accompanied by a transient deformation of the ribose of the adjacent G_5 towards O4′-endo pucker that lasts for about 100 ps before the C3′-endo conformation of the crystal structure is restored (Fig. 6d). Both A_6 and G_5 belong to the U-turn motif and form a stacking platform for the O4′ furanose oxygen of the cleavage-site nucleotide C_{17} in the ground state crystal structure obtained at pH 5.0 (Scott et al. 1996). However, the spontaneous ribose pucker flips in A_6 and G_5 did not lead to conformational changes in either C_{17} or any other of the surrounding nucleotides (Fig. 6d). As mentioned above, the breakage of the hydrogen bond between OP(U_7) and N3-H(U_4) linking the two residues bordering A_6 and G_5, occurred shortly before the flip of the A_6 ribose. Both processes are probably linked and lead to a conformational change in the U-turn. Recently, a conformational change in the catalytic core of the hammerhead ribozyme upon cleavage and affecting the two uridine residues U_4 and U_7 was suggested on the basis of NMR experiments (Simorre et al. 1997).

Structural changes in the hammerhead RNA relevant to catalysis

In all three-dimensional structures of the hammerhead RNA available to date, the cleavage-site 2′-OH is not in a favourable position for the attack at the adjacent phosphate (Fig. 1c) (McKay 1996). However, the finding that the hammerhead ribozyme is able to cleave in the crystal, as demonstrated by warming flash-frozen crystals of an active hammerhead RNA intermediate (Scott et al. 1996), suggests that only a minor change is required to reach a

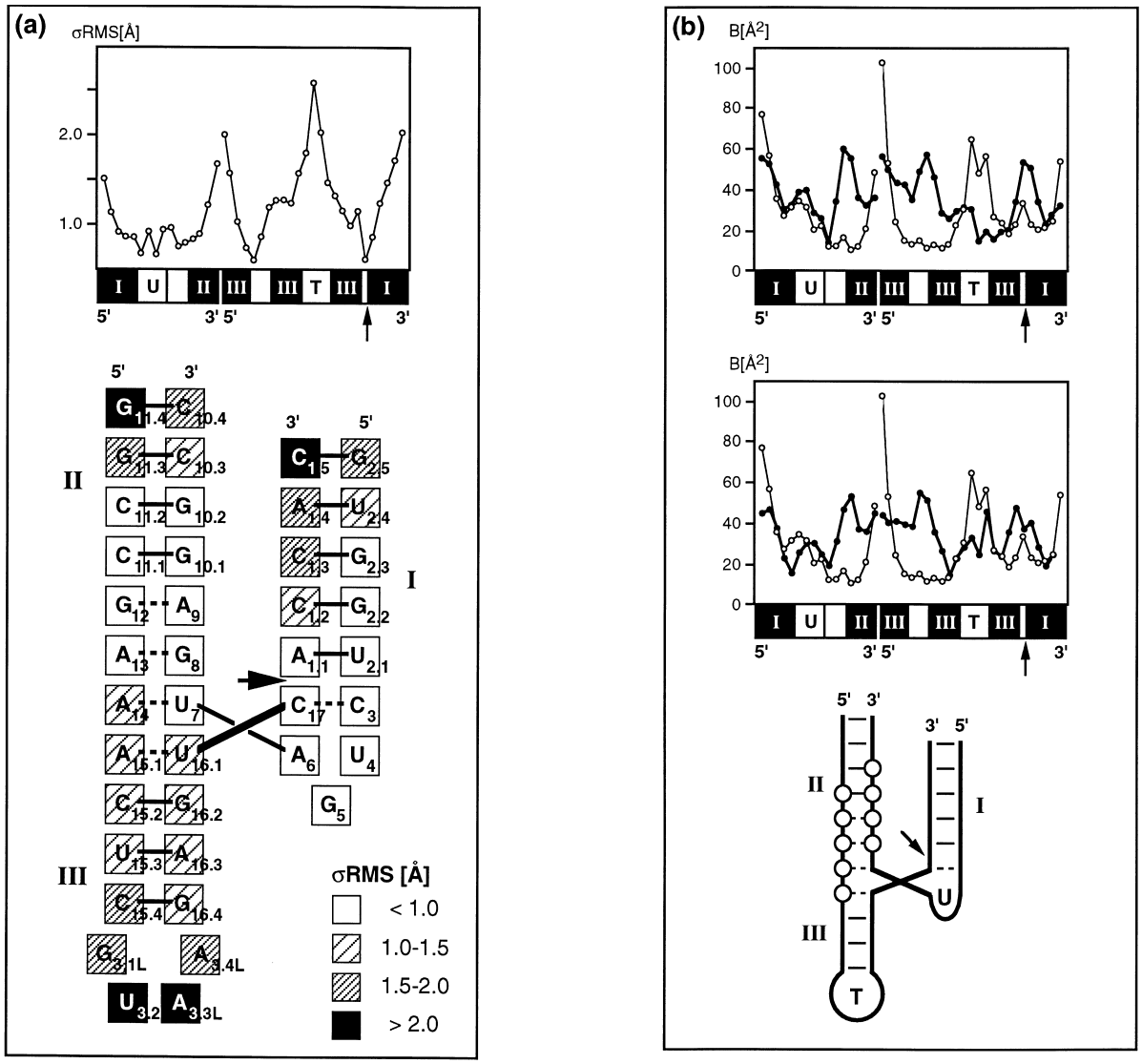

Fig. 6 **a** Flexibility of residues of the hammerhead RNA during a 750 ps MD simulation calculated separately for each nucleotide as the standard deviation of the local RMS deviation (σRMS) during unconstrained calculation. In the *top panel*, the regions of stems I–III, the U-turn (U) and the tetraloop (T) are indicated. In the *bottom panel*, the nucleotides are grouped into four ranges of σRMS coded by different patterns as indicated in the inserted legend. The cleavage site is indicated by an arrow. For the correlation between regions of high flexibility and regions of noteworthy absolute distortions of the crystal structure, compare with Fig. 4b. **b** Per residue *B*-factors calculated from the last 200 ps productive phase of the 750 ps MD simulation (*open circles*) superimposed on the crystallographic *B*-factors (*filled circles*) of the crystal structure of the flash-frozen hammerhead intermediate (*top panel*) (Scott et al. 1996) and of the ribozyme in the ground state (*middle panel*) (Scott et al. 1995). The *bottom panel* shows a schematic representation of the hammerhead secondary structure. Circles indicate residues G_8 to $G_{10.2}$ and $C_{11.1}$ to $A_{15.1}$ where crystallographic *B*-factors deviate markedly from *B*-factors calculated from the MD simulation. *B*-factors calculated on different time periods of the simulation gave similar curves (data not shown). **c** Superposition of per residue *B*-factors from the MD simulation (*open circles*) on the crystallographic *B*-factors (*filled circles*) of a different RNA/DNA hammerhead construct (Pley et al. 1994). The *B*-factors for two different molecules in the unit cell are shown (*top* and *middle panel*). The *bottom panel* outlines the secondary structure of the ribozyme construct of this other crystal structure where stem II is closed by a tetraloop instead of stem III and stems I and III are elongated. *B*-factors were plotted only for the core region (*full lines*) that is identical to the previous hammerhead fold (Fig. 6c). **d** A flip (*arrow*) of the A_6 ribose pucker from C3′-endo to C2′-endo occurred spontaneously during the simulations. The panel shows the recorded pseudorotation phase angle P (Altona and Sundaralingam 1972) for the A_6 ribose and for comparison the values for the neighboring nucleotides U_7, G_5 and U_4. The flip of the A_6 ribose pucker is accompanied by a transient conformational change in the G_5 ribose (*dashed lines*) to the O4′-endo conformation which is restored to the initial C3′-endo pucker after 100 ps

conformation where the cleavage-site C_{17} 2′-OH is in a favourable position for the attack at the adjacent phosphate. Such a conformational change is expected to meet two requirements, namely (i) moving C_{17} 2′-OH closer to the cleavable phosphate than the 3.8 Å observed in the crystal structure, and (ii) positioning C_{17} 2′-OH in a proper orientation for in-line attack at the cleavable phosphate.

We will now extend our previous attempts (Hermann et al. 1997) to uncover the nature of the conformational change that could adjust the position of the cleavage-site

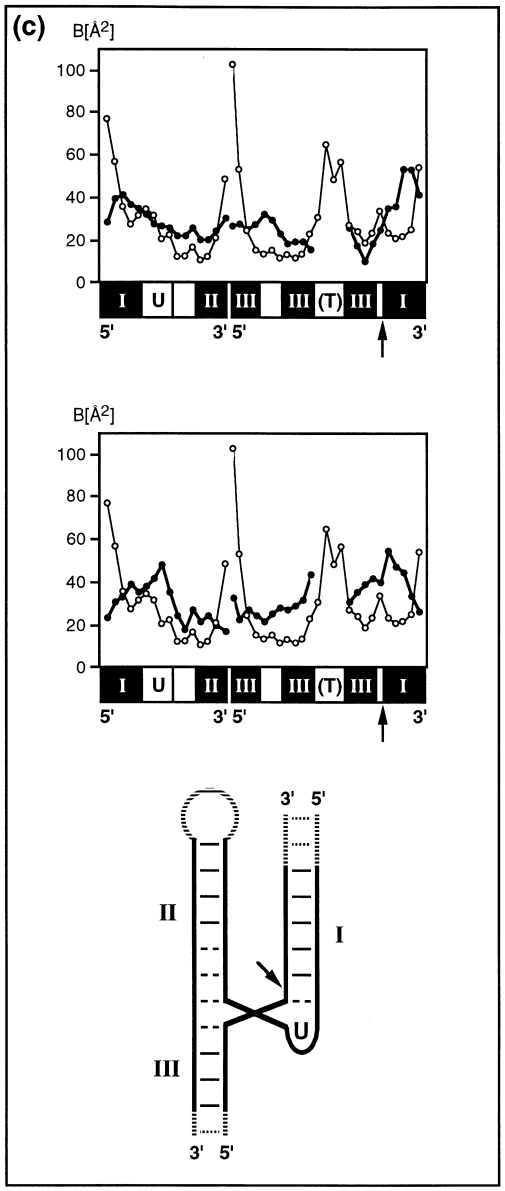

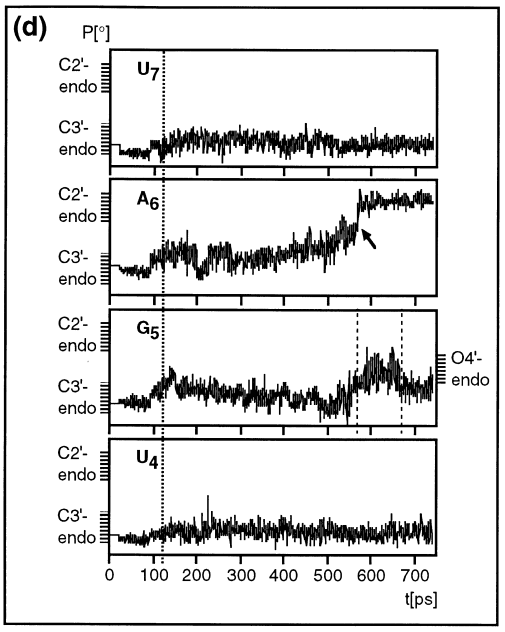

2′-OH. Initially, it was our hope that during the MD calculations the dynamical motions within the RNA at the simulation temperature of 298 K would be sufficient to transiently bring the C_{17} 2′-OH in closer proximity to the attacked phosphate. However, the hammerhead RNA always stayed around the crystal structure and the 2′-OH never approached closer than 3.45 Å to the cleavable phosphate. This distance was reached more frequently in simulations performed at higher temperatures, up to 350 K. As such, this observation is not surprising since the conformational sampling is done around the equilibrium state, from which input of activation energy is required in order to arrive at the transition state. The slow rate of the hammerhead cleavage reaction on the minute timescale (Hertel et al. 1994) could be partially due to such a rate-limiting conformational change. At room temperature, probably only few RNA molecules could be thermally-driven across the activation energy barrier of the conformational change, rendering it a rare process which is beyond the ns time scale of the present MD simulations. Therefore, we externally forced a small change in the RNA during the simulations by inducing a flip of the ribose pucker from C3′-endo to C2′-endo at the C_{17} residue which holds the cleavable 3′-phosphate (Fig. 7a). In concert with the ribose flip, the active-site 2′-OH moved in a proper orientation for in-line attack at the cleavable phosphate and was closer than 3 Å to the attacked phosphorous atom. At the same time, the C_{17} 2′-OH came into hydrogen-bonding distance of the μ-hydroxo-bridged metal cluster of $Mg^{2+}_{(6)}$ and $Mg^{2+}_{(1)}$ (see above) (Fig. 7). The μ-hydroxo-bridged metal cluster could then provide an OH^- ion that is able to activate the 2′-OH nucleophile for attack at the cleavable phosphate. Following on this scenario, a mechanism for the hammerhead catalysis was postulated based on proton shuffling within the hydration shell of the μ-hydroxo-bridged metal cluster where the m-hydroxo bridge transiently stores a proton (Hermann et al. 1997). Thus, a minimal conformational change in the RNA restricted to a single sugar pucker change from C3′-endo to C2′-endo would be sufficient for initiating the cleavage, as also suggested by others (Mei et al. 1989; Setlik et al. 1995).

The ribose flip at the C_{17} residue is a local conformational effect limited to this nucleotide and the neighboring nucleotides $A_{1.1}$, A_6 and G_5 (Fig. 7d,e). Thus, the catalytic site of the hammerhead ribozyme, constituted essentially by the nucleotides of the U-turn (Scott et al. 1996), forms a flexible pocket that can accommodate the conformational change around C_{17} required for initiating the cleavage. A minor but probably essential change is observed at A_6 and G_5 the bases of which tilt up towards the C_{17} residue during the ribose flip (Fig. 7d,e). As pointed out before, A_6 and G_5 are located within the U-turn and form a stacking platform supporting the furanose oxygen of C_{17} in the ground state crystal structure and are stacking also to the base of C_{17} in the crystal structure of the flash-frozen intermediate. It was speculated earlier that the platform of the A_6 and G_5 bases may stabilize the transition state (Scott et al. 1996). The tilting motion of the A_6 and G_5 bases, induced in the MD simulations as a consequence of the forced

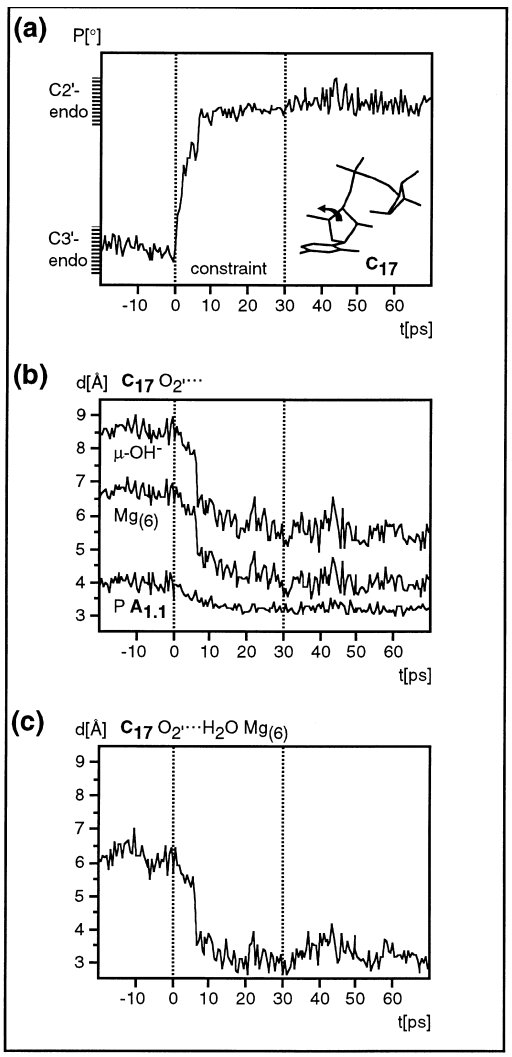

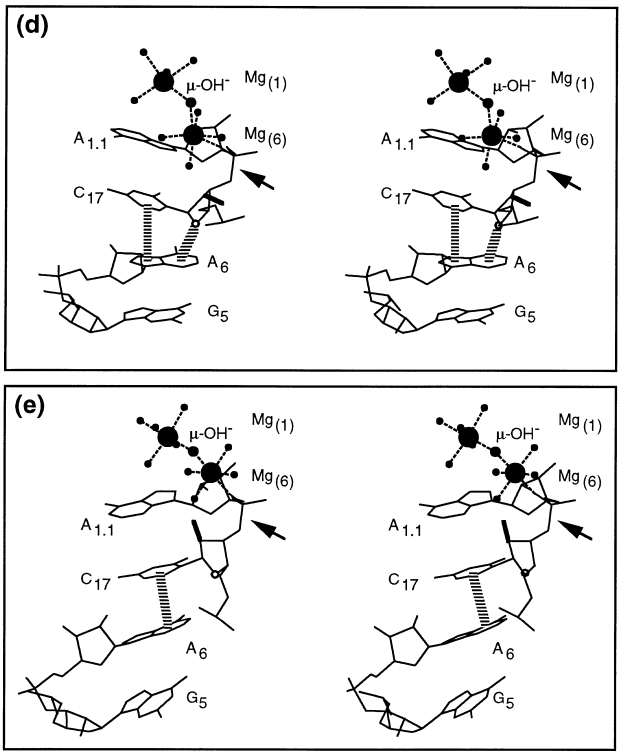

Fig. 7a–e Result of a MD simulation where a flip was induced of the ribose pucker from C3′-endo to C2′-endo at the C_{17} residue which holds the cleavable 3′-phosphate (Hermann et al. 1997). The ribose flip was forced by a harmonical constraint on one of the torsional angles (*v*3, C2′-C3′-C4′-O4′) of the five-membered sugar ring. The constraint was slowly switched on over 10 ps, starting at t = 0, and abruptly switched off after 20 ps of simulation (t = 30, *stippled lines*). **a** Behaviour of the pseudorotation phase angle P for the C_{17} ribose indicating the pucker flip. **b** Changes in distance between the cleavage-site 2′-OH group and, respectively, the attacked phosphorous atom, the Mg^{2+} ion bound to the cleavable phosphate and the μ-hydroxo bridge between $Mg^{2+}_{(6)}$ and $Mg^{2+}_{(1)}$. **c** The C_{17} 2′-OH group also moves into hydrogen-bonding distance of a water molecule in the $Mg^{2+}_{(6)}$ hydration shell during the ribose flip. **d,e** Stereoviews showing the hammerhead active site with the metals $Mg^{2+}_{(6)}$ and $Mg^{2+}_{(1)}$ along with their hydration water and the μ-OH^- ion before **d** and after **e** the ribose pucker flip at C_{17}. The cleavage-site 2′-OH group is enhanced, the cleavable phosphodiester bond indicated by an *arrow*. The base side chains of G_5 and A_6, located within the U-turn, form a stacking platform for C_{17} as indicated by *hatched bars*

ribose flip at C_{17}, ensures a continuous supporting contact of the bottom of the catalytic site with the cleavage site nucleotide C_{17}.

Conclusions

Molecular dynamics calculations using full treatment of the solvent conditions and electrostatic interactions were used to simulate the dynamical behaviour of the hammerhead ribozyme RNA. The RNA stayed close to the starting crystal structure as indicated by an RMS deviation below 2.5 Å after 750 ps of MD simulation. Base pairs and many of the important tertiary interactions within the RNA molecule were retained during the simulations attesting to the performance of the employed protocols and the force field. Tertiary interactions involving 2′-OH groups were found to be less stable, in agreement with previous observations of high rotational mobility of these groups in MD simulations of RNA. The hydrogen bonding dynamics of the two consecutive sheared G · A base pairs suggests a previously unknown in-plane breathing motion of the adenine in G · A pairs. A spontaneous conformational change was observed, involving a flip of the ribose pucker of residues A_6 and G_5, which both act as a supportive stacking platform for the cleavage-site nucleotide C_{17}. The stacking interaction between A_6/G_5 in the U-turn and C_{17} is maintained in constrained simulations where a sugar pucker change from C3′-endo to C2′-endo at C_{17} was forced to reach a conformation where the cleavage reaction is sterically possible. Thus, the MD simulations suggest that an activating conformational change at the cleavage-site nucleotide C_{17} may be coupled or induced by a conformational change in the sugar pucker in residues of the U-turn.

Acknowledgements We thank Peter Kollman and his group at UCSF for making available to us the latest version of the AMBER MD package used in the present study. T. H. is supported by an EMBO long-term fellowship.

References

Altona C, Sundaralingam M (1972) Conformational analysis of the sugar ring in nucleosides and nucleotides. A new description using the concept of pseudorotation. J Am Chem Soc 94:8205–8212

Auffinger P, Westhof E (1996) H-Bond stability in the $tRNA^{Asp}$ anticodon hairpin: 3 ns of multiple molecular dynamics simulations. Biophys J 71:940–954

Auffinger P, Westhof E (1997) Rules governing the orientation of the 2′-hydroxyl group in RNA. J Mol Biol 274:54–63

Åqvist JJ (1990) Ion-water interaction potentials derived from free energy perturbation simulations. Phys Chem 94:8021–8024

Berendsen HJC, Postma JPM, van Gunsteren WF, Dinola A, Haak JR (1984) Molecular dynamics with coupling to an external bath. J Chem Phys 81:3684–3690

Berendsen HJC, Grigera JR, Straatsma TP (1987) The missing term in effective pair potential. J Phys Chem 97:6269–6271

Brion P, Westhof E (1997) Hierarchy and dynamics of RNA folding. Annu Rev Biophys Biomol Struct 26:113–137

Cornell WD, Cieplak P, Bayly CI, Gould IR, Merz KM, Ferguson DM, Spellmeyer DC, Fox T, Caldwell JW, Kollman PA (1995) A second generation force field for the simulation of proteins, nucleic acids and organic molecules. J Am Chem Soc 117:5179–5197

Dahm SC, Uhlenbeck OC (1991) Role of divalent metal ions in the hammerhead RNA cleavage reaction. Biochemistry 30:9464–9469

Dahm SC, Derrick WB, Uhlenbeck OC (1993) Evidence for the role of solvated metal hydroxide in the hammerhead cleavage reaction. Biochemistry 32:13040–13045

Darden TA, York D, Pedersen LG (1993) Particle Mesh Ewald: an N.log(N) method for Ewald sums in large systems. J Chem Phys 98:10089–10092

Engler E, Wipff G (1994) MDDRAW, Strasbourg

Gunsteren WF van, Berendsen HJC (1987) GROMOS 87, Groningen

Hermann T, Auffinger P, Scott WG, Westhof E (1997) Evidence for a hydroxide ion bridging two magnesium ions at the active site of the hammerhead ribozyme. Nucleic Acids Res 25:3421–3427

Hertel KJ, Herschlag D, Uhlenbeck OC (1994) A kinetic and thermodynamic framework for the hammerhead ribozyme reaction. Biochemistry 33:3374–3385

Lee H, Darden TA, Pedersen LG (1995) Molecular dynamics studies of a high resolution Z-DNA crystal. J Chem Phys 102:3830–3834

Long DM, LaRiviere FJ, Uhlenbeck OC (1995) Divalent metal ions and the internal equilibrium of the hammerhead ribozyme. Biochemistry 34:14435–14440

Masquida B, Westhof E (1997). Crystallographic structures of RNA oligoribonucleotides and ribozymes. In: Neidle S (ed) Oxford handbook of nucleic acid structure. London (in press)

McCammon JA, Harvey SC (1987). Dynamics of proteins and nucleic acids. Cambridge University Press, Cambridge

McKay DB (1996) Structure and function of the hammerhead ribozyme: an unfinished story. RNA 2:395–403

Mei HY, Kaaret TW, Bruice TC (1989) A computational approach to the mechanism of self-cleavage of hammerhead RNA. Proc Natl Acad Sci USA 86:9727–9731

Miller JL, Kollman PA (1997) Theoretical studies of an exceptionally stable RNA tetraloop: observation of convergence from an incorrect NMR structure to the correct one using unrestrained molecular dynamics. J Mol Biol 270:436–450

Pearlman DA, Case DA, Caldwell JW, Ross WS, Cheatham TE, DeBolt S, Ferguson D, Seibel G, Singh UC, Weiner PK, Kollman PA (1994) AMBER 4.1, San Francisco, California

Pley HW, Flaherty KM, McKay DB (1994) Three-dimensional structure of a hammerhead ribozyme. Nature 372:68–74

Quigley GJ, Rich A (1976) Structural domains of transfer RNA molecules. Science 194:796–806.

Ryckaert JP, Ciccotti G, Berendsen HJC (1977) Numerical integration of cartesian equations of motion of a system with constraints: molecular dynamics of n-alkanes. J Comput Phys 23:327–336

Scott WG, Klug A (1996) Ribozymes: structure and mechanism in RNA catalysis. Trends Biochem Sci 21:220–224

Scott WG, Finch JT, Klug A (1995) The crystal structure of an all-RNA hammerhead ribozyme: a proposed mechanism for RNA catalytic cleavage. Cell 81:991–1002

Scott WG, Murray JB, Arnold JRP, Stoddard BL, Klug A (1996) Capturing the structure of a catalytic RNA intermediate: the hammerhead ribozyme. Science 274:2065–2069

Setlik RF, Shibata M, Sarma RH, Sarma MH, Kazim AL, Ornstein RL, Tomasi TB, Rein RJ (1995) Modeling of a possible conformational change associated with the catalytic mechanism in the hammerhead ribozyme. J Biomol Struct Dynam 13:515–522

Simorre J-P, Legault P, Hangar AB, Michiels P, Pardi A (1997) A conformational change in the catalytic core of the hammerhead ribozyme upon cleavage of an RNA substrate. Biochemistry 36:518–525

Symons RH (1992) Small catalytic RNAs. Annu Rev Biochem 61:641–671

Takagi, Y, Taira K (1995) Temperature-dependent change in rate-determining step in a reaction catalyzed by a hammerhead ribozyme. FEBS Lett 361:273–276

Thomson JB, Tuschl T, Eckstein F (1996) The hammerhead ribozyme. Nucleic Acids Mol Biol 10:173–196

Tuschl T, Gohlke C, Jovin TM, Westhof E, Eckstein F (1994) A three-dimensional model for the hammerhead ribozyme based on fluorescence measurements. Science 266:785–789

Uhlenbeck O (1987) A small catalytic oligoribonucleotide. Nature 328:596–600

Wahl MC, Sundaralingam M (1995) New crystal structures of nucleic acids and their complexes. Curr Opin Struct Biol 5:282–295

Westhof E, Dumas P, Moras D (1983) Loop stereochemistry and dynamics in transfer RNA. J Biomol Struct Dynam 1:337–355